JACS
JOURNAL OF THE AMERICAN CHEMICAL SOCIETY
Article
pubs.acs.org/JACS

Small-Molecule Inhibition of c-MYC:MAX Leucine Zipper Formation Is Revealed by Ion Mobility Mass Spectrometry

Sophie R. Harvey,[†] Massimiliano Porrini,[‡] Christiane Stachl,[†] Derek MacMillan,[§] Giovanna Zinzalla,*[,⊥] and Perdita E. Barran*[,†]

[†]EastChem School of Chemistry and [‡]School of Physics and Astronomy, University of Edinburgh, Edinburgh EH9 3JJ, U.K.

[§]The School of Chemistry, University College London, London WC1H 0AJ, U.K.

[⊥]Centre for Advanced Cancer Therapies, Microbiology, Tumour and Cell Biology Department, Karolinska Institutet, Nobelsväg 16, 171 77 Stockholm, Sweden

Supporting Information

ABSTRACT: The leucine zipper interaction between MAX and c-MYC has been studied using mass spectrometry and drift time ion mobility mass spectrometry (DT IM-MS) in addition to circular dichroism spectroscopy. Peptides comprising the leucine zipper sequence with (c-MYC-Zip residues 402−434) and without a postulated small-molecule binding region (c-MYC-ZipΔDT residues 406−434) have been synthesized, along with the corresponding MAX leucine zipper (MAX-Zip residues 74−102). c-MYC-Zip:MAX-Zip complexes are observed both in the absence and in the presence of the reported small-molecule inhibitor 10058-F4 for both forms of c-MYC-Zip. DT IM-MS, in combination with molecular dynamics (MD), shows that the c-MYC-Zip:MAX-Zip complex $[M+5H]^{5+}$ exists in two conformations, one extended with a collision cross section (CCS) of 1164 ± 9.3 Å^2 and one compact with a CCS of 982 ± 6.6 Å^2; similar values are observed for the two forms of c-MYC-ZipΔDT:MAX-Zip. Candidate geometries for the complexes have been evaluated with MD simulations. The helical leucine zipper structure previously determined from NMR measurements (Lavigne, P.; et al. *J. Mol. Biol.* **1998**, *281*, 165), altered to include the DT region and subjected to a gas-phase minimization, yields a CCS of 1247 Å^2, which agrees with the extended conformation we observe experimentally. More extensive MD simulations provide compact complexes which are found to be highly disordered, with CCSs that correspond to the compact form from experiment. In the presence of the ligand, the leucine zipper conformation is completely inhibited and only the more disordered species is observed, providing a novel method to study the effect of interactions of disordered systems and subsequent inhibition of the formation of an ordered helical complex.

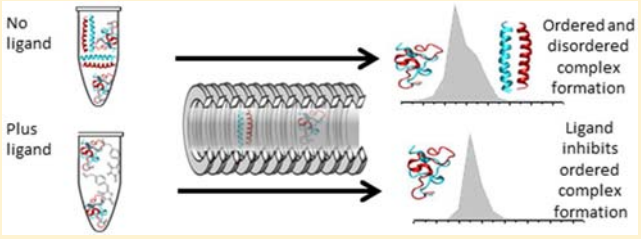

INTRODUCTION

Intrinsically or inherently disordered proteins (IDPs) or intrinsically disordered regions (IDRs) constitute up to 33% of all eukaryotic proteins.[1] They are especially common in signal transduction, where on the order of 75% of proteins involved in signaling pathways in mammals have been predicted to contain long disordered regions[2] and other complex regulatory pathways typical of higher organisms.[3] The lack of defined structure in IDPs can impart a kinetic advantage over ordered proteins, as interactions with other proteins or with DNA couple folding and binding.[4,5] There are a number of different disordered-to-ordered transitions possible for such systems; however, a particularly common transition is from disordered to helical.[6]

IDPs play a critical role in cancer initiation, progression, and metastasis, as well as in other important diseases,[7,8] and although this class of molecular targets is still often considered "undruggable", there is now an imperative to understand the structure−function relationships of IDPs. This must involve the development of methods for the rational design of synthetic agents aimed at the disordered targets and the modulation of their protein−protein interactions with co-factors that regulate the different functions of the IDP. The chemical probes will provide further insight into the signaling pathways controlled by IDPs and their critical role in gene transcription and transrepression and will ultimately drive the development of novel anticancer therapies.[9] To date, the development of chemical approaches in order to design interaction partners for IDPs is in its infancy, and the rational design of IDP ligands is still a challenging task.[10] Biophysical tools that are able to analyze the binding mode of this class of ligands are critical to allow significant progress, in particular the use of *in silico*-based design. Among the few approaches presented to date, it has been suggested that the binding of a small molecule to an IDP can stabilize its disordered state, therefore exploiting the entropic gain of a disordered system to prevent target

Received: July 10, 2012
Published: October 29, 2012

   dx.doi.org/10.1021/ja306519h | *J. Am. Chem. Soc.* 2012, 134, 19384−19392

binding.[9,11] Such an approach has been put forward previously for the IDP, c-MYC (Figure 1A).[11]

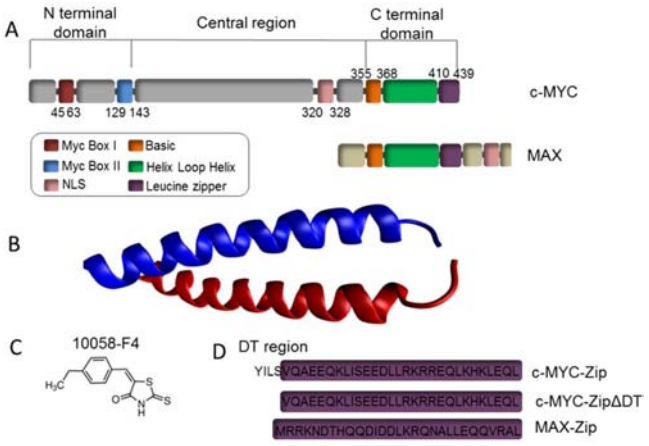

Figure 1. (A) Domain structure of c-MYC and MAX. MYC proteins contain a basic helix–loop–helix leucine zipper (bHLHZip) domain which binds to a similar region on MAX (orange, green, and purple). MYC is 439 amino acid residues long, with the bHLHZip region located at residues 355–439. (B) NMR structure of the c-MYC:MAX leucine zipper structure (PDB file 1A93). (C) Proposed c-MYC inhibitor 10058-F4. (D) Peptides synthesized for this study: the leucine zipper region of MAX and c-MYC, along with a longer c-MYC peptide containing the leucine zipper region and the proposed 10058-F4 target site.

The MYC family of oncoproteins, c-MYC, MYCN, and L-MYC, are transcription factors. Their transcriptional activation and repression of pro-survival and pro-apoptotic target genes are tightly regulated by protein–protein interactions. Following heterodimerization with the obligatory co-factor MAX (Figure 1A), MYC regulates the expression of 10–15% of genes by the recruitment of different co-factors.[12,13] Heterodimerization occurs through the binding of a basic helix–loop–helix leucine zipper (bHLHZip) domain in MYC to a similar region on MAX. The bHLHZip regions of MYC and MAX are intrinsically disordered until they dimerize, when they form a parallel left-handed, four-helix bundle with each monomer composed of two α-helices separated by a loop (Figure 1B).[14] MYC is highly deregulated in a broad range of human cancers, and recently the transgenic mouse models developed in the Evan laboratory have shown that inhibition of MYC transcriptional activity results in rapid tumor regression, with well-tolerated and fully reversible side effects, making MYC inhibitors a valuable pleurotopic target to identify effective cancer therapies.[15,16] However, no anti-MYC drugs are yet clinically available. Hammoudeh et al.[11] have reported a number of c-MYC inhibitors with low micromolar affinity, such as compound 10058-F4 (Figure 1C), which is to our knowledge one of the most potent c-MYC:MAX inhibitors described in the literature. They claim the compounds stabilize the disordered state, preventing MAX dimerization. Three possible binding sites have been proposed for these ligands, with 10058-F4 binding to a seven amino acid stretch of c-MYC that overlaps with the leucine zipper region. In order to probe the interaction of 10058-F4 with the leucine-zipper-forming region of c-MYC, we have synthesized the relevant regions of MAX and c-MYC, including a shorter peptide which consists of the c-MYC leucine zipper region but does not contain the additional amino acids which make up the drug target region. (Figure 1D).

Due to the flexibility of IDPs, traditional experimental approaches to characterizing their structures and interactions with ligands are limited.[17,18] Ion mobility mass spectrometry (IM-MS) is, however, gaining credibility as a tool for structural analysis of peptides.[19−21] One of the advantages of IM-MS over more traditional structural characterization techniques is that it can easily separate and distinguish between different conformations of the same species. The use of IM-MS to study IDPs[22,23] in addition to peptide–ligand interactions[24] is particularly attractive since it can both separate bound and unbound states and probe conformational changes. Canon et al. utilized IM-MS to study the unfolded-to-folded transition of the salivary protein IB5 upon binding to a model target, EgCG,[25] highlighting how such techniques can provide detailed insight into the conformational distribution of complex multiconformational mixtures. Berezovskaya et al. utilized MS and IM-MS to study the effect of ligand binding on peptide structure, examining the effect of metal binding in zinc-finger peptides.[26] Wyttenbach et al. also utilized IM-MS in combination with molecular dynamics (MD) and other MS techniques to study the interactions of metal ions with the cyclic peptide oxytocin.[27] Their results indicated that the complexes formed between oxytocin and transition metals and detected in the gas phase were similar to their solution-phase counterparts, highlighting how these gas-phase techniques can be applied to the study of peptide–ligand complexes to provide insight into these complex systems.

The simplest configuration of IM-MS utilizes traditional linear drift-time ion mobility coupled with mass spectrometry (DT-IM-MS).[28,29] In DT-IM-MS, ions are introduced into a drift cell of known length, filled with a known buffer gas at known pressure. A weak electric field is applied across the drift cell, which causes the ions to drift through the cell, while their progress is slowed by collisions with the buffer gas. The mobility (K) of an ion in the drift cell is based not only on its mass and charge but also on its shape, or rotationally averaged collision cross section (CCS, Ω). The mobility of an ion can be determined as the ratio of the drift velocity (v_d) and applied electric field (E). It is then possible to determine the CCS on the basis of a modified version of eq 1,[30]

$$K_0 = \frac{3ze}{16N}\left(\frac{2\pi}{\mu k_B T}\right)^{1/2}\frac{1}{\Omega} \quad (1)$$

Where K_0 is the reduced mobility, z is the ion charge state, e is the elementary charge, N is the gas number density, μ is the reduced mass of the ion-neutral pair, k_B is the Boltzmann constant, and T is the gas temperature. In order to gain further insight into the conformations adopted by biomolecules in the gas phase, it is possible to carry out comparisons between the experimental CCSs and theoretical CCSs, obtained either through computational predictions or using coordinates obtained from NMR or crystal studies.[31−33]

We have employed DT IM-MS to probe conformational changes of an intrinsically disordered oncoprotein, c-MYC, that orders on binding to its dimerization partner MAX.[34,35] Specifically, DT IM-MS allows us to examine the disordered free, disordered bound, and the configured bound states. The latter two are co-incident in m/z space but distinguished by their differing conformations. Furthermore, we probe the effect of a weak inhibitor on the equilibrium between these states.

dx.doi.org/10.1021/ja306519h | J. Am. Chem. Soc. 2012, 134, 19384−19392

EXPERIMENTAL SECTION

Synthesis of Peptides. Peptide synthesis was carried out using Rink amide MBHA resin for the production of peptide carboxamides (loading = 0.64 mmol/g). The resin and all Fmoc amino acids were purchased from Novabiochem. Mass spectra, used to confirm the identity of assembled sequences, were obtained on a Waters uPLC/SQD-LC series electrospray mass spectrometer. Liquid chromatography−mass spectrometry (LC-MS) was performed using a gradient of 5−95% acetonitrile containing 0.1% trifluoroacetic acid (TFA) over 10 min (flow rate of 0.6 mL/min). Semipreparative high-performance liquid chromatography (HPLC) was performed using a Phenomenex LUNA C18 column and a gradient of 10−90% acetonitrile containing 0.1% TFA over 50 min (flow rate of 4.0 mL/min). All other chemical reagents were obtained from Sigma. For further details on the synthetic procedure, see the Supporting Information.

Mass Spectrometry and Ion Mobility Mass Spectrometry. Nanoelectrospray ionization (n-ESI) was utilized for all MS and DT IM-MS experiments. Sample solutions were ionized through a potential applied to a thin platinum wire inserted in a glass capillary. Nanoelectrospray tips were made in-house using thin-walled glass capillaries (i.d. 0.5 mm) and a Flaming/Brown micropipet puller (Sutter Instrument Co., Novato, CA).

Mass Spectrometry. MS experiments were performed on a Q-ToF II instrument (Waters, Manchester, UK). Peptide samples c-MYC-Zip plus MAX-Zip, and c-MYC-ZipΔDT plus MAX-Zip, were prepared in 20 mM ammonium acetate with 20% acetonitrile at a 1:1 ratio, with each peptide present at a concentration of 125 μM. The peptide mix plus 10058-F4 (Sigma Aldrich, Gillingham, UK), prepared in acetonitrile, samples were prepared at an equimolar concentration with all components present at a concentration of 125 μM. Samples were incubated at 37 °C in a digital dry bath (Jencons-PLS, East Grinstead, UK) and were analyzed after 15 min, 1 h, 3 h, and 6 h. Identical tuning conditions were employed for each sample: capillary voltage 1.6 kV, cone voltage 23 V, source temperature 80 °C, collision energy 4.9, and pusher period 125 μs.

Ion Mobility Mass Spectrometry. DT IM-MS measurements were performed on a Q-TOF instrument (Micromass UK Ltd.) that was modified in-house to carry out separations based on an ion's mobility, enabling the temperature-dependent CCSs to be determined. This is possible via the inclusion of a 5.1 cm long copper drift cell and supplementary ion optics situated post source but before the quadrupole analyzer. The instrument and its operation have been described in detail elsewhere.[36] Single peptide samples were prepared at a concentration of 125 μM in 20 mM ammonium acetate. Mixed peptide solutions were prepared at a 1:1 ratio with each peptide present at a concentration of 125 μM in 20 mM ammonium acetate with 20% acetonitrile and incubated at 37 °C for 1 h before analysis. In the presence of the ligand, samples were incubated for 3 h. In all cases, repeats were performed on three different days. Identical tuning conditions were employed for each sample: capillary voltage 1.6 kV, cone voltage 56 V, source temperature 80 °C, and pusher period 130 μs. The temperature and pressure of helium in the drift cell were approximately 28 °C and 4.0 Torr, respectively. Measurements were made at eight different drift voltages from 60 to 15 V. Ion arrival time distributions were recorded by synchronization of the release of ions into the drift cell with mass spectral acquisition. Using the theory described above, the mobility of each ion of interest was obtained from a plot of average arrival time versus pressure/temperature, and from this the rotationally averaged collision cross sections for each resolvable species at a given charge state were obtained using eq 1. Each experiment was performed in triplicate.

MS data obtained on both the Q-TOF II and the ion mobility capable Q-TOF instruments were comparable.

Molecular Modeling. The initial .pdb coordinate file was downloaded from the Research Collaboratory for Structural Bioinformatics (RCSB) databank Web site, PDB code 1A93, which is the NMR structure of c-MYC:MAX heterodimeric leucine zipper. Monomeric and dimeric species were built from these coordinates, splitting them into monomers and adding the four-residue stretch YILS to create the c-MYC-Zip. The rotationally averaged CCSs of the two heterodimeric leucine zippers, c-MYC-Zip:MAX-Zip and c-MYC-ZipΔDT:MAX-Zip, were calculated from these initial coordinates files, minimized *in vacuo* using the trajectory method implemented in MOBCAL code.[37] To derive the CCSs of monomeric and dimeric disordered species, the following simulated annealing (SA) procedure was used: Initial minimization was performed, followed by dynamics for 60 ps at 800 K. Gradual exponential stepwise cooling from 800 to 0 K was then carried out with 2 ps per step, followed by a final minimization. This procedure was carried out 500 times for monomers and 1000 times for dimers. Chirality restraints were used to keep the angles at biological equilibrium values, as during the dynamics at 800 K they might incur a chirality inversion.

The MD engine SANDER of the Amber10 software package was utilized to propagate trajectories *in vacuo*, implementing the Amber99 SB-ILDN force field.[38] All bonds involving hydrogen atoms were kept constrained at their equilibrium values using the SHAKE algorithm,[39] and a time step of 1.0 fs was utilized. An "infinite" radial cutoff (r_c = 999 Å) was used to evaluate the nonbonded interactions, and the temperature was kept constant through the weak-coupling algorithm[40] during the dynamics propagation. In the case of the dimers, the following potential well was applied between the monomers' centers of mass in order to prevent their complete dissociation during the "hot" dynamics:

$$V(r) = \begin{cases} 0, & \text{if} \quad r < r_{La} \\ \frac{1}{2}k(r - r_{La})^2, & \text{if} \quad r_{La} \le r < r_{Lb} \\ k(r - r_{Lb}), & \text{if} \quad r \ge r_{Lb} \end{cases} \qquad (2)$$

where r is the distance between the monomers' centers of mass, r_{La} = 107.0 Å and r_{Lb} = 107.5 Å are the distances at which harmonic and linear potentials start being effective, respectively, and k = 500 is the force constant for the harmonic potential (measured in kcal mol^{-1} Å^{-2}) and the slope of the linear potential (measured in kcal mol^{-1} Å^{-1}). Essentially the functional form of eq 2 represents a potential well in which the monomers are able to move and the breadth of which (ca. 107 Å) is just larger than the distance between the centers of mass of the two monomers in their fully extended conformation and aligned in succession along their longitudinal axis.

Circular Dichroism. Single peptide solutions were prepared at 25 μM in 10 mM ammonium acetate buffer, pH 6.8. The mixed peptide solutions were prepared at a 1:1 ratio with a total protein concentration of 25 μM in 10 mM ammonium acetate buffer, in the absence and in the presence of the ligand, 12.5 μM concentration. All CD spectra were recorded using a quartz cuvette with a 1 mm path length (Hellma, Essex, UK) on a J-810 spectropolarimeter (Jasco, Essex, UK). Spectra were recorded at 25 °C, over the range 190−290 nm, at a rate of 10 nm min^{-1}. Five scans were acquired for each sample and averaged to give the final spectrum. Buffer or buffer plus ligand in the absence of peptide was used as a reference, and the background was subtracted for such. The spectra were smoothed using the Savitzky−Golay algorithm, with a convolution width of 25. The secondary structure content was estimated using the CDSSTR algorithm on the DICHROWEB server.[41−43]

RESULTS

n-ESI of the Peptides. MS incubation experiments were performed on the c-MYC-Zip and MAX-Zip peptides, as well as an additional c-MYC peptide, c-MYC-ZipΔDT (Figure 1D). c-MYC-ZipΔDT consists of the leucine zipper region but does not contain the additional four amino acids (YILS) which are thought to be involved in binding to 10058-F4. Spectra were obtained via n-ESI from solutions buffered with ammonium acetate (pH 6.8). In order to best preserve conformations and complexes present in solution, the key source parameters were optimized, in particular the capillary, sample, and extractor cone voltages. The spectra of the mixed peptide solutions show

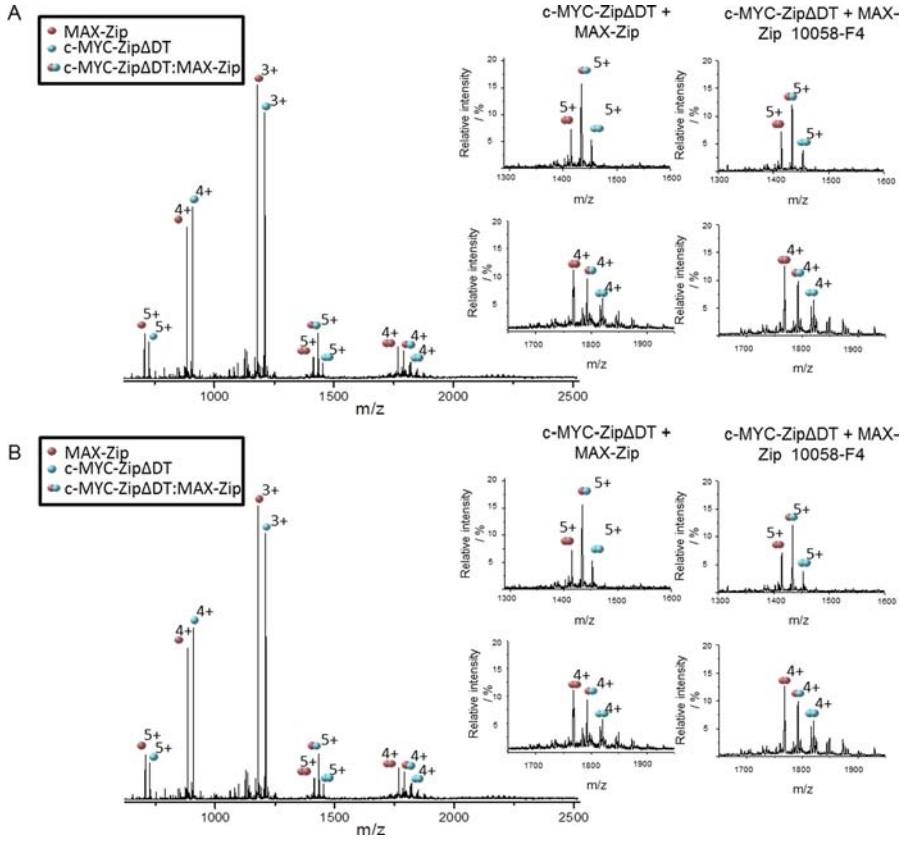

Figure 2. Mass spectra recorded after 3 h incubation at 37 °C of (a, top) c-MYC-Zip plus MAX-Zip (1:1) [Inset: magnified region of the spectra showing the c-MYC:MAX-Zip complexes in the absence and presence of 10058-F4] and (b, bottom) c-MYC-ZipΔDT plus MAX-Zip [Inset: magnified region of the spectra showing the c-MYC-ZipΔDT:MAX-Zip complex in the absence and in the presence of 10058-F4].

relatively narrow charge state distributions of the monomeric species, typically over the range $[M+3H]^{3+}$ to $[M+5H]^{5+}$ for each of the peptides (Figure 2). The theoretical PI values for c-MYC-Zip, c-MYC-ZipΔDT, and MAX are 6.79, 6.76, and 8.36, with net charges of 0, 0, and 2+, respectively. We typically see ions populating lower charge states than the number of protonatable sites, suggesting that not all potential chargeable sites are accessible for protonation, although it is also feasible that deprotonation of some carboxylic groups has occurred. We also observe, at lower intensity, homodimers of c-MYC-Zip, c-MYC-ZipΔDT, and MAX-Zip, at charge states 4+ and 5+. In addition, the c-MYC-Zip:MAX-Zip and c-MYC-ZipΔDT:-MAX-Zip heterodimers were also observed, as $[M+4H]^{4+}$and $[M+5H]^{5+}$, where M represents the complex.

Effect of 10058-F4 on Complex Formation. Upon the addition of stoichiometric amounts of 10058-F4, no ligand−peptide or ligand−complex species was observed for either c-MYC peptide, despite a reported K_d = 5.3 μM[11] to c-MYC, which should be sufficient to preserve via n-ESI.[44] Additionally, previous work has highlighted that truncated segments of c-MYC bind the ligand 10058-F4 with similar affinity.[45] These experiments were repeated with a 5:1 excess of ligand, and still no ligand−peptide complex was observed. For both c-MYC peptides, a decrease in the intensity of the $[M+5H]^{5+}$ complex species was observed in the presence of the ligand, with the largest decrease in complex signal observed after 3 h of incubation at 37 °C (see Supporting Information, Table S1). However, an increase in the $[M+4H]^{4+}$ species was also observed. Therefore, based on the MS experiments alone, addition of the ligand 10058-F4 does not significantly affect the total equilibrium between free peptide and complex, but it affects the charge state distribution, a point that shall be returned to below.

Effect of Solution and Desolvation Conditions. A number of solution and desolvation conditions were employed in attempts to observe the 10058-F4:c-MYC-Zip complex. Initially, the effect of varying the solution conditions was probed by changing both the concentration of the ammonium acetate buffer, over the range 10−100 mM, and the pH of the solution, using 20 mM ammonium acetate over the pH range from 9.8 to 2.8. In all cases, neither the 10058-F4:c-MYC-Zip complex nor the 10058-F4:c-MYC-Zip:MAX-Zip complex was observed. Addition of the ligand itself does not cause any significant shift in the pH of the sample; however, it is less soluble at low pH, crashing out of solution below 2.8 at concentrations of 125 μM. A number of desolvation conditions were also probed, including the effect of capillary voltage, the potential applied in order to ionize and desolvate the sample. The capillary voltage was applied over the range 1.3−2.0 kV; however, the charge applied does not appear to affect our ability to transmit or observe the ligand complexes. Furthermore, the effect of cone voltage was investigated over the range 10−40 V, but even with the gentlest conditions, no ligand complex could be observed. Finally, solvent vapor exposure during ionization was implemented, which has previously been shown to stabilize weak gas-phase peptide−ligand interactions,[46] but again no peptide−ligand complexes were observed. It is significant that we were unable to observe the c-MYC-Zip:10058-F4 complex under any of the conditions tested here, as previous work has shown that the preservation of

dx.doi.org/10.1021/ja306519h | J. Am. Chem. Soc. 2012, 134, 19384−19392

hydrophobic interactions is indeed possible in the gas phase.[47,48] We would therefore infer from this that the K_d of the ligand is greater than has been quoted in earlier studies, and any ligand binding in solution is too weak to be preserved during desolvation and ionization, even under very gentle source conditions.

Effect of 10058-F4 on Complex Conformations. Following DT IM-MS experiments, rotationally averaged CCSs were determined for each species observed (see Table 1).

Table 1. Experimental[a] and Theoretical[b] Collisional Cross Sections

species		CCS, Å^2 exptl	CCS, Å^2 theor
MAX-Zip	$[1M+2H]^{2+}$		560
	$[1M+4H]^{4+}$	565 ± 1.5	
	$[1M+3H]^{3+}$	554 ± 5.9	
c-MYC-ZipΔDT	1M		592
	$[1M+4H]^{4+}$	629 ± 4.2	
	$[1M+3H]^{3+}$	595 ± 5.1	
	$[1M+2H]^{2+}$	453 ± 11.3	
c-MYC-Zip	1M		627
	$[1M+4H]^{4+}$	711 ± 2.1	
	$[1M+3H]^{3+}$	649 ± 3.3	
	$[1M+2H]^{2+}$	479 ± 7.8	
c-MYC-ZipΔDT:MAX-Zip	$[1M+2H]^{2+}$		918
			1162
	$[1M+5H]^{5+}$	947 ± 3.3	
		1136 ± 11.8	
	$[1M+4H]^{4+}$	906 ± 2.6	
c-MYC-Zip:MAX-Zip	$[1M+2H]^{2+}$		962
			1247
	$[1M+5H]^{5+}$	982 ± 6.6	
		1164 ± 9.3	
	$[1M+4H]^{4+}$	923 ± 8.5	

[a]Experimental CCSs listed here were determined from the single peptide and mixed peptide solutions in the absence of the ligand. [b]Theoretical CCSs were determined either from simulated annealing or from NMR coordinates, for the extended complex.

Experimental CCSs are compared to theoretical CCSs obtained from a SA procedure or from the NMR structure of the MYC:MAX leucine zipper (extended heterodimer).[14] In the SA procedure for each stored minimized structure, the rotationally averaged CCS was determined, and the representative structures (Figures 3 and 5) were chosen, selecting the lowest energy species among those having a CCS "close" to the peak position of the distributions.

Considering a window of 10.0 Å^2 centered at the CCS distribution peak position, ensembles of structures (ca. 100 for the monomers and ca. 160 for the dimers) could be determined and used to derive the secondary structure contents of each species via DSSP[49] (as implemented in Amber10 package). The DSSP algorithm enables the secondary structure of the amino acids in a peptide or protein to be assigned on the basis of the atomic-resolution coordinates of the species; the resulting trends for the three peptides and the heterodimeric peptides obtained through SA are displayed in Figure 4.

For monomeric peptides, experimental CCSs show good agreement with values obtained for the low-energy modeled candidate structures, which are compact and possess little secondary structure. In the presence of the ligand, the CCSs of

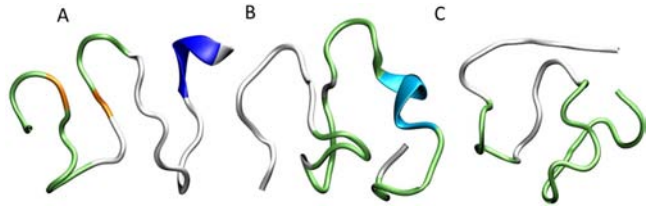

Figure 3. Theoretically predicted structures obtained through simulated annealing of (A) c-MYC-ZipΔDT, (B) c-MYC-Zip, and (C) MAX-Zip. The colors refer to the secondary structure as follows: green, white, orange, blue, and cyan refer to turn, coil, isolated bridge, 3−10-helix, and α-helix, respectively.

all monomeric species remain the same within experimental error. The MAX-Zip homodimer exists as a single, compact conformation, whereas the c-MYC-Zip homodimer is observed as a single, extended conformation. However, in both cases the CCSs do not change upon addition of 10058-F4.

For the heterodimeric complex, in the absence of ligand, two conformations are observed for the $[M+5H]^{5+}$ species (Figure 5 top). The more extended of these corresponds to the calculated CCS for the leucine zipper dimer derived from the NMR coordinates as annotated in Figure 5. The earlier arriving conformer corresponds to a more compact complex, with a CCS similar to the most visited CCS value of the low-energy candidates determined through the SA approach. The difference in width observed for the arrival time distributions (ATDs) obtained experimentally as opposed to the distribution obtained through the SA procedure is likely due to both diffusion and conformational heterogeneity; that is to say; the structures will exist in a conformational family of similar structures. We can here surmise that the complex exists in solution as both disordered (potentially the encounter complex) and structured forms and that both forms can be transferred into the gas phase.

By contrast, in the presence of the ligand after 3 h of incubation, only one conformation is observed for the $[M+5H]^{5+}$ heterodimeric species, the more compact and disordered species (Figure 5 bottom). This provides compelling evidence for the inhibition of the helical leucine zipper structure in the presence of the ligand. Incubation of ligand and c-MYC-Zip:MAX-Zip for 1 h was also sufficient to remove the extended species. The complex is also observed as a $[M+4H]^{4+}$ ion, which presents as a single conformation, similar in CCS to the disordered complexes provided by SA. The shape of the ATD for the $[M+4H]^{4+}$ complex does not alter in the presence of the ligand; however, the structure does appear to shift to a slightly lower CCS (Figure 6A), suggesting the ligand promotes a more compact form to be favored. The more compact form may favor a lower charge state in the gas phase since less protonatable sites will be accessible, and in part this observation explains the relative increase of the $[M+4H]^{4+}$ species in the presence of the ligand.

A further MD simulation was carried out on the c-MYC-Zip:MAX-Zip leucine zipper-like complex to determine its stability at 300 K. The SANDER MD engine of Amber11 was used to propagate the trajectories, implementing AMBER99SB-ildn force field with a time step of 2 fs, keeping bonds involving hydrogen atoms constrained at their equilibrium value via SHAKE algorithm. After thermalizing and equilibrating the leucine zipper in a truncated octahedral box of explicit water TIP3P (with ca. 9780 water molecules and 2 Cl^- ions to

dx.doi.org/10.1021/ja306519h | J. Am. Chem. Soc. 2012, 134, 19384−19392

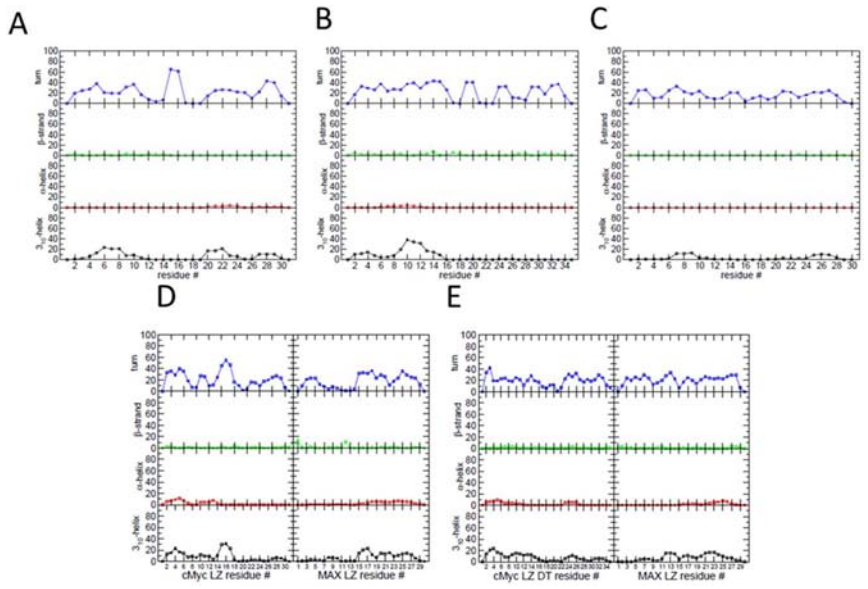

Figure 4. Secondary structure contents in percentage for (A) c-MYC-ZipΔDT, (B) c-MYC-Zip, (C) MAX-Zip, (D) c-MYC-ZipΔDT:MAX-Zip, and (E) c-MYC-Zip:MAX-Zip.

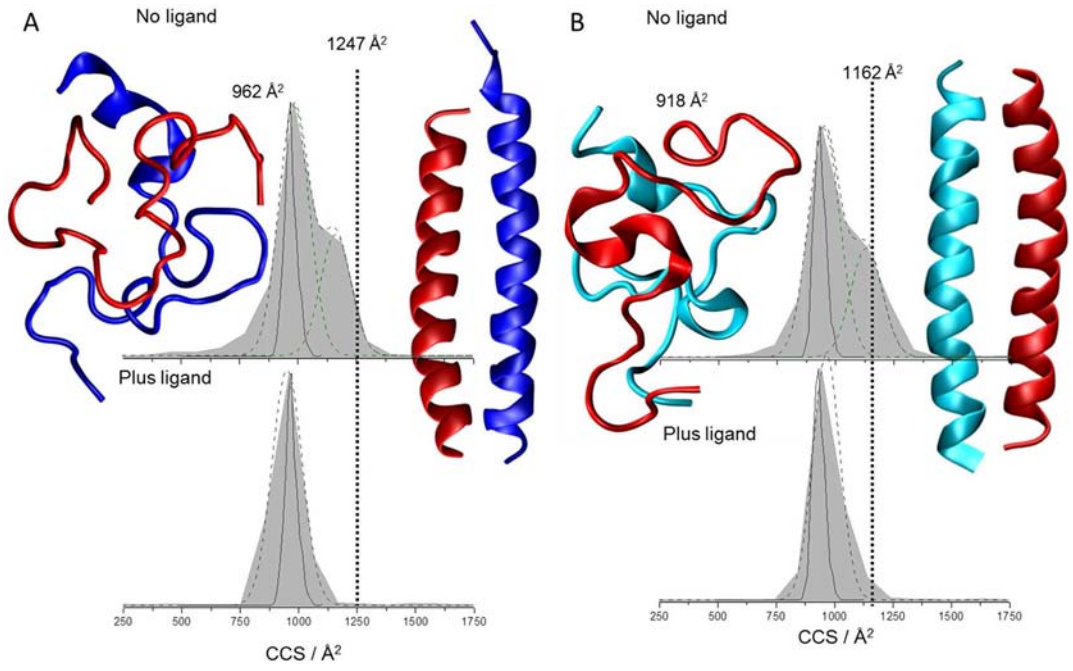

Figure 5. CCS distributions derived from arrival time distributions at a drift voltage of 45 V for the complex $[M+5H]^{5+}$ ions. Results in the absence of ligand (after 1 h incubation at 37 °C) and in the presence of the ligand 10058-F4 (after 3 h incubation at 37 °C) are shown in the top and bottom panels, respectively. Profiles for the predicted conformation from simulated annealing (solid lines) and from NMR structures (vertical dotted line) are displayed together with experimental fitted curves (dashed lines): (A) c-MYC-zip:MAX-Zip and (B) c-MYC-ZipΔDT:MAX-Zip.

neutralize the system) at T = 300 K and P = 1 atm, a 10 ns production run was carried out. After the water molecules were stripped out, 100 sample structures were stored (1 every 100 ps) along the obtained trajectory and minimized *in vacuo*. The CCS for each resulting structure was then calculated, and the average was found to be 1124 Å^2. This value is in very close agreement with our experimental value of 1164 Å^2, highlighting that this helix−helix interaction is stable *in vacuo* at the temperature employed during the experimental procedure.

For the c-MYC-ZipΔDT peptide, similar observations were made through DT IM-MS. In the absence of the ligand, the $[M+5H]^{5+}$ exists as two conformations, a compact conformation and a more extended conformation, consistent with the CCS predicted for the leucine zipper. In the presence of the ligand, the more extended conformation is again inhibited, suggesting this ligand 10058-F4 is not as specific as previously reported (Figure 5B). As with c-MYC-Zip:MAX-Zip, the c-MYC-ZipΔDT:MAX $[M+4H]^{4+}$ complex exists as a single conformation which is not affected by the addition of the 10058-F4 (Figure 6B).

Considering the Solution-Phase Conformations. The helical content of these peptides, in solution conditions

dx.doi.org/10.1021/ja306519h | J. Am. Chem. Soc. 2012, 134, 19384−19392

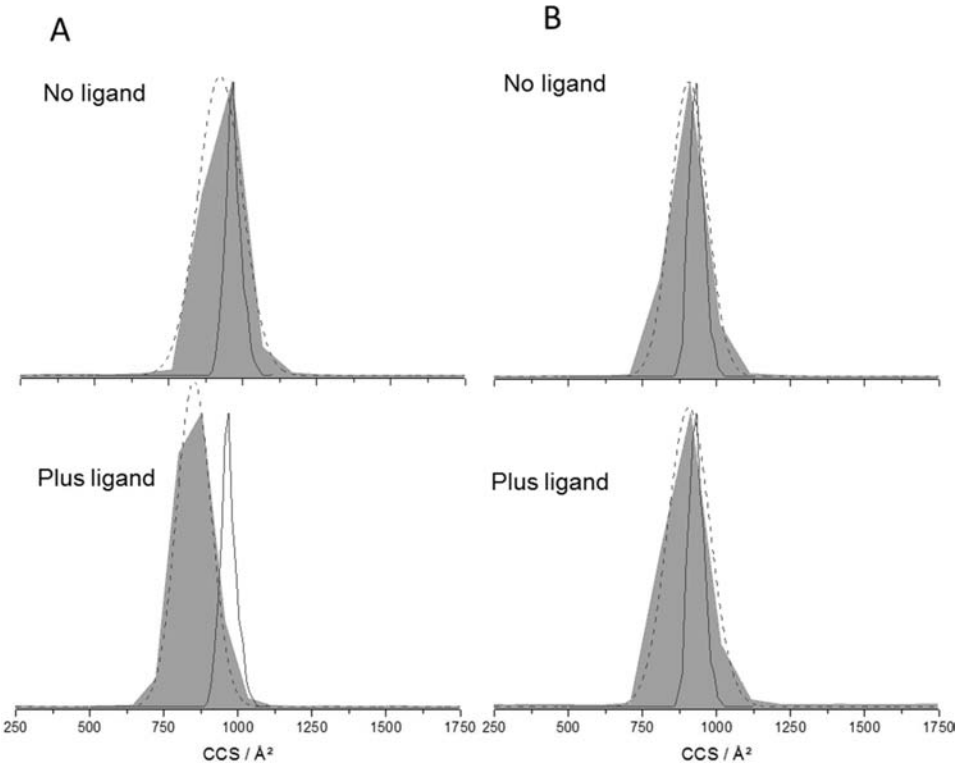

Figure 6. CCS distributions derived from arrival time distributions at a drift voltage of 45 V for the complex $[M+4H]^{4+}$ ions. Results in the absence of ligand (after 1 h incubation at 37 °C) and in the presence of the ligand 10058-F4 (after 3 h incubation at 37 °C) are shown in the top and bottom panels, respectively. Profiles for the predicted conformation from simulated annealing (solid lines) are displayed together with experimental fitted curves (dashed lines): (A) c-MYC-Zip:MAX-Zip and (B) c-MYC-ZipΔDT:MAX-Zip.

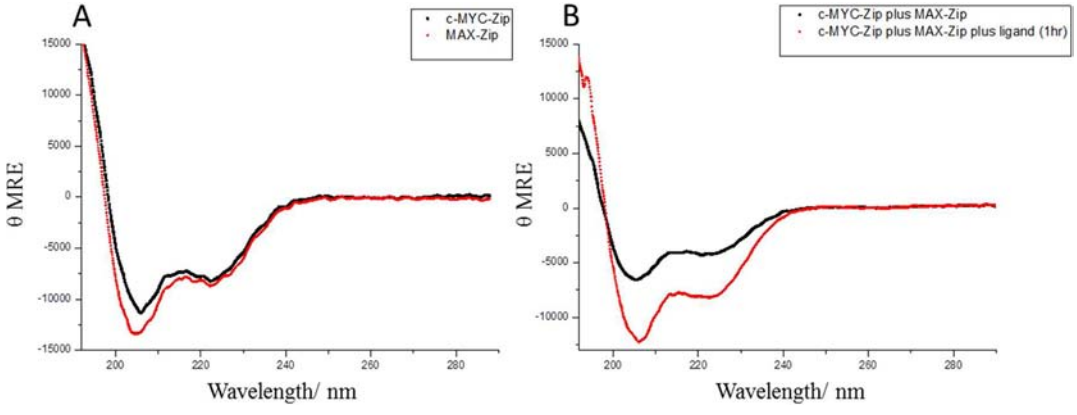

Figure 7. CD spectra for (A) c-MYC-Zip and MAX-Zip and (B) 1:1 MY-Zip:MAX-Zip in the absence and in the presence of the ligand 10058-F4.

reflecting those used for the DT IM-MS experiments, was assessed using circular dichroism (CD). We find, in contrast to the report of Hammoudeh et al., that c-MYC-Zip and MAX-Zip as individual peptide solutions possess some helicity (Figure 7A), although we have taken slightly differing regions of the c-MYC:MAX interaction domain.[11] From CD experiments it is not possible to determine if this helicity is due to the monomeric peptides or their homodimers. Indeed, both the monomer and dimer structures we have generated via molecular modeling, while being mainly disordered, do have some helical content, as shown by DSSP analysis (Figure 4). Additionally, the 1:1 mixed peptide solution also shows a helical signature, which upon incubation with the ligand 10058-F4 is observed to *increase* slightly (Figure 7B). Additionally, at pH 9.8 and 2.8, a helical signature is still observed for the 1:1 mixed peptide solution both in the presence and in the absence of the ligand, suggesting that pH over this range does not significantly affect the solution secondary structure. It appears that CD provides ambiguous results in this study of a multicomponent, conformationally dynamic system.

DISCUSSION

Does the Postulated Drug Target Region Have an Effect? c-MYC-Zip versus c-MYC-ZipΔDT. Two different length c-MYC peptides were studied, both containing the leucine zipper region, but c-MYC-Zip also contained the previously identified 10058-F4 binding site. However, our studies showed no significant difference between the c-MYC-Zip and c-MYC-ZipΔDT peptides with respect to ligand binding, despite the fact that c-MYC-ZipΔDT does not contain

dx.doi.org/10.1021/ja306519h | J. Am. Chem. Soc. 2012, 134, 19384−19392

the 10058-F4 binding region. This leads us to infer that the ligand is not as specific as previously reported, nor does the ligand bind as strongly. Indeed, a recent study utilizing metadynamics simulations on a 10 amino acid stretch of c-MYC containing the identified drug target region, c-$MYC_{402-412}$, suggests that the ligand binding to c-MYC is driven primarily by weak, nonspecific interactions with hydrophobic patches.[50] If the interactions are indeed primarily nonspecific, this could help explain why we see no difference between the c-MYC peptide containing the binding site and that which does not. For the heterodimers we see a loss of the extended conformations with the addition of ligand, and in the case of the longer c-Myc a further compaction of the compact form. The CCSs of the homodimeric complexes do not alter in the presence of the ligand, which indicates that the ligand does not interact with them in solution, and supports the specificity of the ligand for the disordered heterodimer.

What Is the Effect of Charge? It is interesting to note the difference in complex conformation between the two charge states observed: namely, the complex exists as a single conformational family for the $[M+4H]^{4+}$ charge state but as two distinct conformational families for the $[M+5H]^{5+}$ charge state. We have assigned likely candidates for each of these structures using MD simulations. The $[M+5H]^{5+}$ complex exists as both a compact species, assigned as a disordered complex, and a more extended complex, similar to the coiled-coiled leucine zipper complex, while the $[M+4H]^{4+}$ complex exists only as a compact, potentially disordered complex. The fact that the leucine zipper-like conformation is only observed at the higher charge state is unsurprising; helical structures with their side chains sticking out would be more likely to exist in higher charge states,[51] whereas the disordered complex could exist at lower charge states due to self-solvation of the peptides, leading to a more compact complex. Indeed, visual examination of the disordered complex shows that the chargeable residues reside mostly in the core of the complex; this structure would be likely to present at lower charge states. In comparison, the leucine zipper structure cannot undergo the same self-solvation of charges and is therefore less likely to be observed at lower charge states. We have also seen that the ligand induces a compaction of the gas-phase complex, which is most marked for the c-MYC-Zip:MAX-Zip complex, where the $[M+4H]^{4+}$ species increases intensity and decreases CCS, suggesting that the looser form seen in the absence of ligand and as the $[M+5H]^{5+}$ species may be en route to zipper formation.

SUMMARY

Solution-based methods for quantifying small changes in secondary structure for principally disordered systems cannot provide the clear distinction between components that DT IM-MS has done here. We are able to separate monomers from homodimers, and from heterodimers, and to determine the conformation of each. We have shown that the c-MYC:MAX leucine zipper can exist in two conformations, one of which is compact and hence likely disordered, and a second which corresponds to an extended and potentially "coiled-coil" structure. This form is removed in the presence of a known c-MYC:MAX inhibitor, suggesting that 10058-F4 interacts with the disordered state and prevents zipper formation. This mass spectrometry-based approach to the effect of a drug candidate on a protein−protein interaction has great promise as a tool to answer critical biological questions and to develop novel therapeutic agents. Future work and further optimization could allow the equilibrium between disordered and ordered structures to be elucidated and applied to help determine to the solution-phase equilibrium.

ASSOCIATED CONTENT

Supporting Information

Further details on the synthetic procedure used to manufacture the peptides, MS incubation experiment results, and further DT IM-MS experiments. This material is available free of charge via the Internet at http://pubs.acs.org.

AUTHOR INFORMATION

Corresponding Author

Giovanna.Zinzalla@ki.se; Perdita.Barran@ed.ac.uk

Notes

The authors declare no competing financial interest.

ACKNOWLEDGMENTS

The Schools of Chemistry and Physics at the University of Edinburgh are thanked for an award of a EPSRC DTA studentship to S.R.H. M.P. is employed on a BBRSC grant BB/H013636/1, but the BBRSC have not yet funded this work directly. G.Z. acknowledges support from the Centre for Advanced Cancer Therapies of Karolinska Institutet (69 701 013 Zinzalla G/Temacentrum). We acknowledge Ali Murtuza, Danting Shen, and Savina Hortarea for early discussions on c-MYC as part of their M.Sc. research methods exercise in the School of Chemistry, University of Edinburgh.

REFERENCES

(1) Fink, A. L. *Curr. Opin. Struct. Biol.* **2005**, *15*, 35−41.
(2) Dunker, A. K.; Silman, I.; Uversky, V. N.; Sussman, J. L. *Curr. Opin. Struct. Biol.* **2008**, *18*, 756−764.
(3) Dunker, A. K.; Brown, C. J.; Lawson, J. D.; Iakoucheva, L. M.; Obradović, Z. *Biochemistry* **2002**, *41*, 6573−6582.
(4) Wright, P. E.; Dyson, H. J. *Curr. Opin. Struct. Biol.* **2009**, *19*, 31−38.
(5) Dyson, H. J.; Wright, P. E. *Nat. Rev. Mol. Cell. Biol.* **2005**, *6*, 197−208.
(6) Fuxreiter, M.; Simon, I.; Friedrich, P.; Tompa, P. *J. Mol. Biol.* **2004**, *338*, 1015−1026.
(7) Iakoucheva, L. M.; Brown, C. J.; Lawson, J. D.; Obradović, Z.; Dunker, A. K. *J. Mol. Biol.* **2002**, *323*, 573−584.
(8) Metallo, S. J. *Curr. Opin. Chem. Biol.* **2010**, *14*, 481−488.
(9) Cheng, Y.; LeGall, T.; Oldfield, C. J.; Mueller, J. P.; Van, Y.-Y. J.; Romero, P.; Cortese, M. S.; Uversky, V. N.; Dunker, A. K. *Trends Biotechnol.* **2006**, *24*, 435−442.
(10) Dunker, A. K.; Uversky, V. N. *Curr. Opin. Pharmacol.* **2010**, *10*, 782−788.
(11) Hammoudeh, D. I.; Follis, A. V.; Prochownik, E. V.; Metallo, S. J. *J. Am. Chem. Soc.* **2009**, *131*, 7390−7401.
(12) Fernandez, P. C.; Frank, S. R.; Wang, L.; Schroeder, M.; Liu, S.; Greene, J.; Cocito, A.; Amati, B. *Genes Dev.* **2003**, *17*, 1115−1129.
(13) Li, Z.; Van Calcar, S.; Qu, C.; Cavenee, W. K.; Zhang, M. Q.; Ren, B. *Proc. Natl. Acad. Sci. U.S.A.* **2003**, *100*, 8164−8169.
(14) Lavigne, P.; Crump, M. P.; Gagne, S. M.; Hodges, R. S.; Kay, C. M.; Sykes, B. D. *J. Mol. Biol.* **1998**, *281*, 165−181.
(15) Sodir, N.; Evan, G. *J. Biol.* **2009**, *8*, 77.
(16) Soucek, L.; Whitfield, J.; Martins, C.; Finch, A.; Murphy, D.; Sodir, N.; Karnezis, A.; Swigart, L.; Nasi, S.; Evan, G. *Nature* **2008**, *455*, 679−683.
(17) Mittag, T.; Forman-Kay, J. D. *Curr. Opin. Struct. Biol.* **2007**, *17*, 3−14.
(18) Uversky, V. N.; Oldfield, C. J.; Dunker, A. K. *Annu. Rev. Biophys.* **2008**, *37*, 215−246.

(19) Harvey, S. R.; MacPhee, C. E.; Barran, P. E. *Methods* **2011**, *54*, 454−461.
(20) Kanu, A. B.; Dwivedi, P.; Tam, M.; Matz, L.; Hill, H. H. *J. Mass Spectrom.* **2008**, *43*, 1−22.
(21) Joly, L.; Antoine, R.; Albrieux, F.; Ballivian, R.; Broyer, M.; Chirot, F.; Lemoine, J.; Dugourd, P.; Greco, C.; Mitrić, R.; Bonačić-Koutecký, V. *J. Phys. Chem. B* **2009**, *113*, 11293−11300.
(22) Bernstein, S. L.; Liu, D.; Wyttenbach, T.; Bowers, M. T.; Lee, J. C.; Gray, H. B.; Winkler, J. R. *J. Am. Soc. Mass Spectrom.* **2004**, *15*, 1435−1443.
(23) Pagel, K.; Natan, E.; Hall, Z.; Fersht, A. R.; Robinson, C. V. *Angew. Chem., Int. Ed.* **2012**, *9*, 201203047.
(24) Hyung, S. J.; Robinson, C. V.; Ruotolo, B. T. *Chem. Biol.* **2009**, *16*, 382−390.
(25) Canon, F.; Ballivian, R.; Chirot, F.; Antoine, R.; Sarni-Manchado, P.; Lemoine, J. R. M.; Dugourd, P. *J. Am. Chem. Soc.* **2011**, *133*, 7847−7852.
(26) Berezovskaya, Y.; Armstrong, C. T.; Boyle, A. L.; Porrini, M.; Woolfson, D. N.; Barran, P. E. *Chem. Commun.* **2011**, *47*, 412−414.
(27) Wyttenbach, T.; Liu, D.; Bowers, M. T. *J. Am. Chem. Soc.* **2008**, *130*, 5993−6000.
(28) K. B. McAfee, J.; Edelson, D. *Proc. Phys. Soc.* **1963**, *81*, 382.
(29) Hogg, A. M.; Kebarle, P. *J. Chem. Phys.* **1965**, *43*, 449−456.
(30) Mason, E. A.; McDaniel, E. W. *Transport Properties of Ions in Gases*; Wiley-VCH Verlag GmbH & Co. KGaA: Berlin, 2005; pp 551−560.
(31) Knapman, T. W.; Berryman, J. T.; Campuzano, I.; Harris, S. A.; Ashcroft, A. E. *Int. J. Mass Spectrom.* **2010**, *298*, 17−23.
(32) McCullough, B. J.; Eastwood, H.; Clark, D. J.; Polfer, N. C.; Campopiano, D. J.; Dorin, J. A.; Maxwell, A.; Langley, R. J.; Govan, J. R. W.; Bernstein, S. L. *Int. J. Mass Spectrom.* **2006**, *252*, 180−188.
(33) Wu, C.; Murray, M. M.; Bernstein, S. L.; Condron, M. M.; Bitan, G.; Shea, J.-E.; Bowers, M. T. *J. Mol. Biol.* **2009**, *387*, 492−501.
(34) Blackwood, E. M.; Eisenman, R. N. *Science* **1991**, *251*, 1211−1217.
(35) Blackwood, E. M.; Lüscher, B.; Eisenman, R. N. *Genes Dev.* **1992**, *6*, 71−80.
(36) McCullough, B. J.; Kalapothakis, J.; Eastwood, H.; Kemper, P.; MacMillan, D.; Taylor, K.; Dorin, J.; Barran, P. E. *Anal. Chem.* **2008**, *80*, 6336−6344.
(37) Shvartsburg, A. A.; Schatz, G. C.; Jarrold, M. F. *J. Chem. Phys.* **1998**, *108*, 2416−2423.
(38) Lindorff-Larsen, K.; Piana, S.; Palmo, K.; Maragakis, P.; Klepeis, J. L.; Dror, R. O.; Shaw, D. E. *Proteins: Struct., Funct. Bioinf.* **2010**, *78*, 1950−1958.
(39) Ryckaert, J.-P.; Ciccotti, G.; Berendsen, H. J. C. *J. Comput. Phys.* **1977**, *23*, 327−341.
(40) Berendsen, H. J. C.; Postma, J. P. M.; Vangunsteren, W. F.; Dinola, A.; Haak, J. R. *J. Chem. Phys.* **1984**, *81*, 3684−3690.
(41) Whitmore, L.; Wallace, B. A. *Nucleic Acids Res.* **2004**, *32*, W668−W673.
(42) Whitmore, L.; Wallace, B. A. *Biopolymers* **2008**, *89*, 392−400.
(43) Johnson, W. C. *Proteins: Struct., Funct. Genet.* **1999**, *35*, 307−312.
(44) Yin, S.; Xie, Y.; Loo, J. A. *J. Am. Soc. Mass Spectrom.* **2008**, *19*, 1199−1208.
(45) Follis, A. V.; Hammoudeh, D. I.; Wang, H.; Prochownik, E. V.; Metallo, S. J. *Chem. Biol.* **2008**, *15*, 1149−1155.
(46) Hopper, J. T. S.; Sokratous, K.; Oldham, N. J. *Anal. Biochem.* **2012**, *421*, 788−790.
(47) Liu, L.; Michelsen, K.; Kitova, E. N.; Schnier, P. D.; Klassen, J. S. *J. Am. Chem. Soc.* **2010**, *132*, 17658−17660.
(48) Liu, L.; Kitova, E. N.; Klassen, J. S. *J. Am. Soc. Mass Spectrom.* **2011**, *22*, 310−318.
(49) Kabsch, W.; Sander, C. *Biopolymers* **1983**, *22*, 2577−2637.
(50) Michel, J.; Cuchillo, R. *PLoS One* **2012**, *7*, e41070 DOI: 10.1371/journal.pone.0041070.
(51) Hoaglund-Hyzer, C. S.; Counterman, A. E.; Clemmer, D. E. *Chem. Rev.* **1999**, *99*, 3037−3080.